International Journal of Biological Macromolecules 341 (2026) 150224

Contents lists available at ScienceDirect

International Journal of Biological Macromolecules

journal homepage: www.elsevier.com/locate/ijbiomac

Differential roles of proteasome and autophagy in α-synuclein and E46K oligomer clearance: insight into the modulatory effects of the dopamine metabolite DOPAC

Manuela Leri [a], Philipp Trolese [b,c], Ilenia Inciardi [b], Patrizia Polverino de Laureto [b], Monica Bucciantini [a,*]

[a] Department of Experimental and Clinical Biomedical Sciences, University of Florence, Viale Morgagni 50, 50134, Florence, Italy
[b] Department of Pharmaceutical and Pharmacological Sciences, University of Padova, Via Marzolo 5, 35131, Padova, Italy
[c] Department of Neuroscience, Biomedicine and Movement Sciences, University of Verona, Piazzale Ludovico Antonio Scuro 10, 37124, Verona, Italy

ARTICLE INFO

Keywords:
DOPAC
α-Synuclein
E46K mutation
Proteasome degradation
macroautophagy

ABSTRACT

The build-up of misfolded α-synuclein (Syn) proteins plays a key role in diseases such as Parkinson's disease. Here, we compared the cytotoxicity and intracellular processing of wild-type and E46K mutant Syn aggregates in SH-SY5Y neuroblastoma cells and investigated the modulatory effects of the dopamine metabolite, 3,4-dihydroxyphenylacetic acid (DOPAC). E46K aggregates displayed markedly higher toxicity than wild-type counterparts, promoting mitochondrial dysfunction and elevated reactive oxygen species (ROS) production in a time-dependent manner. This effect is consistent with the mutation's higher affinity for cellular membranes, which fosters early and sustained aggregate–membrane interactions. Strikingly, co-incubation with DOPAC during aggregation significantly reduced both toxicity and oxidative stress in wild-type and E46K aggregates. DOPAC shifted Syn into less fibrillogenic conformations, favouring smaller oligomers that were less membrane-active and more effectively processed by cellular clearance systems. Mechanistic studies revealed that E46K/DOPAC aggregates were preferentially degraded via the ubiquitin–proteasome system (UPS), as proteasome inhibition with MG132 enhanced toxicity and intracellular accumulation. In contrast, autophagy inhibition by chloroquine paradoxically reduced toxicity, indicating redirection toward UPS-mediated degradation. Analysis of lysosomal markers showed that DOPAC-containing aggregates colocalized with LAMP1 but not LAMP2A, suggesting processing through macroautophagy rather than chaperone-mediated autophagy. Furthermore, p62 accumulation, indicative of impaired autophagic flux, was evident with untreated aggregates but absent when DOPAC was present. Overall, our results demonstrate that DOPAC reshapes the biophysical and toxicological properties of Syn aggregates, especially E46K species, by promoting less harmful oligomers and enhancing proteostatic clearance. These findings highlight DOPAC as a promising modulator of Syn aggregation and pathology.

1. Introduction

α-Synuclein (Syn) is a presynaptic protein with multifaceted roles in neuronal physiology. Traditionally, it is known as a regulator of synaptic vesicle dynamics, balancing vesicle clustering and SNARE-complex chaperoning to fine-tune neurotransmitter release. Beyond this canonical function, emerging evidence indicates that Syn also acts as a modulator of mRNA stability through interactions with processing bodies (P-bodies), linking it to post-transcriptional gene regulation [1]. This dual functionality places Syn at a critical intersection between synaptic activity and gene expression homeostasis.

Pathogenic mutations such as E46K exemplify the disease relevance of Syn. This mutation causes early-onset Parkinson's disease (PD) characterized by severe cognitive and motor deficits, along with neuroimaging patterns resembling those of advanced idiopathic PD [2]. Such findings underscore how Syn dysfunction, whether by mutation or misfolding, can perturb neuronal integrity across molecular, structural, and functional levels.

In healthy cells, the accumulation of misfolded or aggregated proteins is prevented by two major degradation systems: the

* Corresponding author.
E-mail address: monica.bucciantini@unifi.it (M. Bucciantini).

https://doi.org/10.1016/j.ijbiomac.2026.150224
Received 17 November 2025; Received in revised form 4 January 2026; Accepted 10 January 2026
Available online 13 January 2026

ubiquitin–proteasome system (UPS) and the autophagy–lysosomal pathway (ALP). The UPS primarily degrades soluble and misfolded Syn species through ubiquitin tagging and subsequent 26S proteasome-mediated proteolysis [3]. In contrast, autophagy, particularly macroautophagy and chaperone-mediated autophagy (CMA), eliminates larger aggregates and organelles that escape proteasomal clearance [4,5]. CMA selectively recognizes Syn species via a KFERQ-like motif, targeting them for lysosomal degradation. This division of labour establishes a finely tuned proteostasis network, whose disruption leads to Syn accumulation, oxidative stress, and neuroinflammation, hallmarks of PD and related synucleinopathies [6,7]. Indeed, PD neurons often display reduced levels of autophagy-related proteins (ATGs) and impaired ubiquitin signaling, reflecting a general decline in clearance capacity [8,9].

Syn aggregation creates a self-reinforcing proteotoxic cycle. Oligomeric Syn can be degraded by the proteasome but paradoxically impair proteasome activity by sequestering essential subunits [10–12]. Simultaneously, lysosomal degradation becomes overwhelmed as Syn's KFERQ motif competes for import machinery. Experimental inhibition of these systems reveals their bidirectional crosstalk: proteasome blockade (e.g., with epoxomicin) increases Syn levels but enhances compensatory CMA, whereas macroautophagy inhibition (e.g., with 3-methyladenine) suppresses proteasomal activity [13]. Combined inhibition of both systems synergistically worsens Syn accumulation and neuronal death, confirming their non-redundant and cooperative roles in maintaining neuronal proteostasis [14]. These findings position Syn at the nexus of synaptic function and proteostasis, where its mutations or pathological aggregation disrupt vesicular trafficking and mRNA regulation while overwhelming the compensatory mechanisms between UPS and ALP. Understanding this interplay not only elucidates the molecular underpinnings of PD but also suggests that therapeutic strategies aimed at reinforcing both degradation pathways may break the cycle of proteostasis failure and mitigate neurodegeneration.

Beyond proteostasis disruption, Syn aggregation exerts toxicity through direct interactions with cellular membranes. The N-terminal α-helical region binds preferentially to anionic phospholipids [15,16], promoting lipid extraction [17], vesicle tubulation [18], and membrane destabilization [19]. These effects compromise cellular integrity and synaptic function. Importantly, such binding is dynamic and influenced by the lipid environment and cytosolic factors, suggesting a context-dependent modulation of Syn's membrane activity [20]. The convergence of proteostasis collapse and membrane remodeling represents a dual mechanism of neurodegeneration in PD.

The dopamine metabolite 3,4-dihydroxyphenylacetic acid (DOPAC) plays a distinctive role in modulating Syn aggregation. Unlike dopamine aldehyde (DOPAL), which promotes toxic Syn oligomer formation, DOPAC inhibits fibril growth and stabilizes smaller, no toxic oligomers such as dimers and trimers [21,22]. These DOPAC-induced oligomers generate fewer reactive oxygen species (ROS) and exhibit reduced cytotoxicity compared to typical Syn aggregates. Moreover, DOPAC-stabilized Syn species can activate autophagic pathways, suggesting that DOPAC not only alters aggregation dynamics but also enhances cellular clearance mechanisms. Interestingly, these oligomers display altered membrane interactions, which may affect their recognition by proteostatic systems and reduce membrane perturbation.

This paper aims to elucidate the role of DOPAC in promoting the clearance of Syn aggregates, highlighting its potential as an endogenous modulator capable of redirecting Syn aggregation toward less toxic forms while enhancing their degradation. By influencing aggregation dynamics and proteostatic pathways, DOPAC may contribute to restoring cellular homeostasis and slowing neurodegeneration in Parkinson's disease.

2. Material and methods

2.1. Cell culture conditions and treatments

SH-SY5Y cells were cultured at 37 °C in a humidified incubator under a 5.0% CO2 atmosphere in 50:50 HAM: DMEM culture medium supplemented with 10% foetal bovine serum, 3.0 mM glutamine, 100 units/mL penicillin and 100 μg/mL streptomycin. The cells were exposed for 4, 24 or 72 h to vehicle or to 5 μM Syn samples, obtained as described below.

2.2. Syn and E46K purification and aggregates preparation

The expression and the purification of the recombinant proteins α-Synuclein and its E46K mutant were conducted in *E. coli* BL21 and BL21-Gold cells respectively following a procedure previously described [23]. Protein identity and integrity were assessed by ESI-mass spectrometry (MS).

The complexes between Syn and E46K with DOPAC were obtained by mixing the protein with the catechol in 1:5 ratio and by incubating for 72 h. The species were characterized by circular dichroism, Thioflavin assay and transmission electron microscopy.

2.3. Mitochondria functionality

The MTT reagent (3-(4,5-dimethylthiazol-2-yl)-2,5-diphenyltetrazolium bromide (Sigma-Aldrich, St. Louis, MO, USA) was added to SH-SY5Y cells seeded in 96-well plates (1×10^4 cells/well) at a final concentration of 0.5 mg/mL. After incubation for 2 h at 37 °C, formazan crystals formed from MTT by the reducing activity of mitochondrial dehydrogenases were dissolved with 100 μL solubilizing solution (DMSO) and the absorbance of the blue formazan resulting from MTT reduction was read at 595 nm using a Biotek Synergy 1H spectrophotometric plate reader.

2.4. Reactive oxygen species measurements

The probe 2′,7′-dichlorofluorescein diacetate, acetyl ester (CM-H2 DCFDA; Sigma-Aldrich) was added at a final concentration of 10 mM to SH-SY5Y cells plated in 96-well plates (1×10^4 cells/well). After 1 h, fluorescence values were read at 538 nm using a Biotek Synergy 1H spectrophotometric plate reader.

2.5. Confocal immunofluorescence

Sub-confluent SH-SY5Y cells grown on glass coverslips were treated with Syn aggregates at a final concentration of 5.0 μM (monomeric protein concentration) for 4 h and 24 h and then washed with PBS. Nuclei were stained with HOECHST 33342 for 30 min at 37 °C. LAMP1, LAMP2, p62 and Syn proteins were stained with mouse monoclonal anti-LAMP1 (1:500) (SC20011, Santa Cruz Biotechnology), mouse monoclonal anti-LAMP2 (Santa-Cruz) rabbit polyclonal anti-SQSTM1/p62 (1:500, GTX100685, GeneTex, USA) and rabbit polyclonal anti-Syn antibody (1:500, PA5–85791, Invitrogen, USA) followed by anti-mouse Alexa Fluor 488-conjugated secondary antibodies (green channel) and anti-rabbit Alexa Fluo 568-conjugated secondary antibodies (red channel), respectively. Cell fluorescence was imaged using a Leica TCS SP8 confocal scanning microscope (Leica, Mannheim, DE, USA). Observations were made with a Leica HC PL Apo CS2 X63 oil immersion objective. Images reconstruction, signal fluorescence quantification and Manders' overlap coefficients were obtained using Image J Fiji software [24].

2.6. STED microscopy

STED xyz images were acquired using an SP8 STED 3× confocal

microscope (Leica Microsystems, Mannheim, Germany). Cell nuclei were stained with HOECHST 33342 for 30 min at 37 °C. Cell membranes were stained with 0.01 mg/mL WGA, tetramethylrhodamine conjugate (W849, Thermo Fisher Scientific). Syn was detected with a 1:500 diluted mouse monoclonal anti-αSyn antibody (sc12767, Santa Cruz Biotechnology) and a 1:500 Alexa-Fluor 514-conjugated anti-rabbit secondary antibody (A-31555, Thermo Fisher Scientific). Fluoromount-G™ (00–4958-02, Fisher Scientific) was used as a mounting medium. Images were captured using a Leica HC PL APO CS2 100×/1.40 oil STED White objective. Gated pulsed STED was applied with Alexa-Fluor 514 fluorophore. Collected images were deconvolved using Huygens Professional software (Scientific Volume Imaging B.V., Hilversum, The Netherlands; version 18.04) and analyzed using Leica Application Suite X (LAS X) software (Leica) to generate 3D reconstructions. Size particles were evaluated in 5 images for each sample and their size/shape measured using the FiJi software (https://imagej.net/imaging/particle-analysis; [24]).

2.7. Circular dichroism (CD) spectroscopy

CD spectra of Syn and its mutant oligomers (5 μM) formed in the presence (1:5 protein/DOPAC) and in the absence of DOPAC were recorded in PBS on a Jasco (Tokyo, Japan) J-710 spectropolarimeter using a 0.1 cm pathlength quartz cuvette. An average of five scans was acquired for each sample. The contribution of the buffer was removed from spectra. The mean residue ellipticity [θ] (degree cm^2 $dmol^{-1}$) was calculated from the formula $[\theta] = (\theta_{obs}/10)$ (MRW/lc), where θ_{obs} is the observed ellipticity in degrees; MRW is the mean residue molecular weight of the protein; l the optical path length in cm; and c is the protein concentration in g/mL. Protein concentrations were determined by absorption measurements at 280 nm using a double-beam Jasco spectrophotometer. The molar absorptivity at 280 nm was 5960 cm^{-1} M^{-1}, as evaluated from the protein amino acid composition [25].

2.8. Negative staining transmission electron microscopy (TEM)

A drop of the sample solution (5 μL) was placed on a Butvar-coated

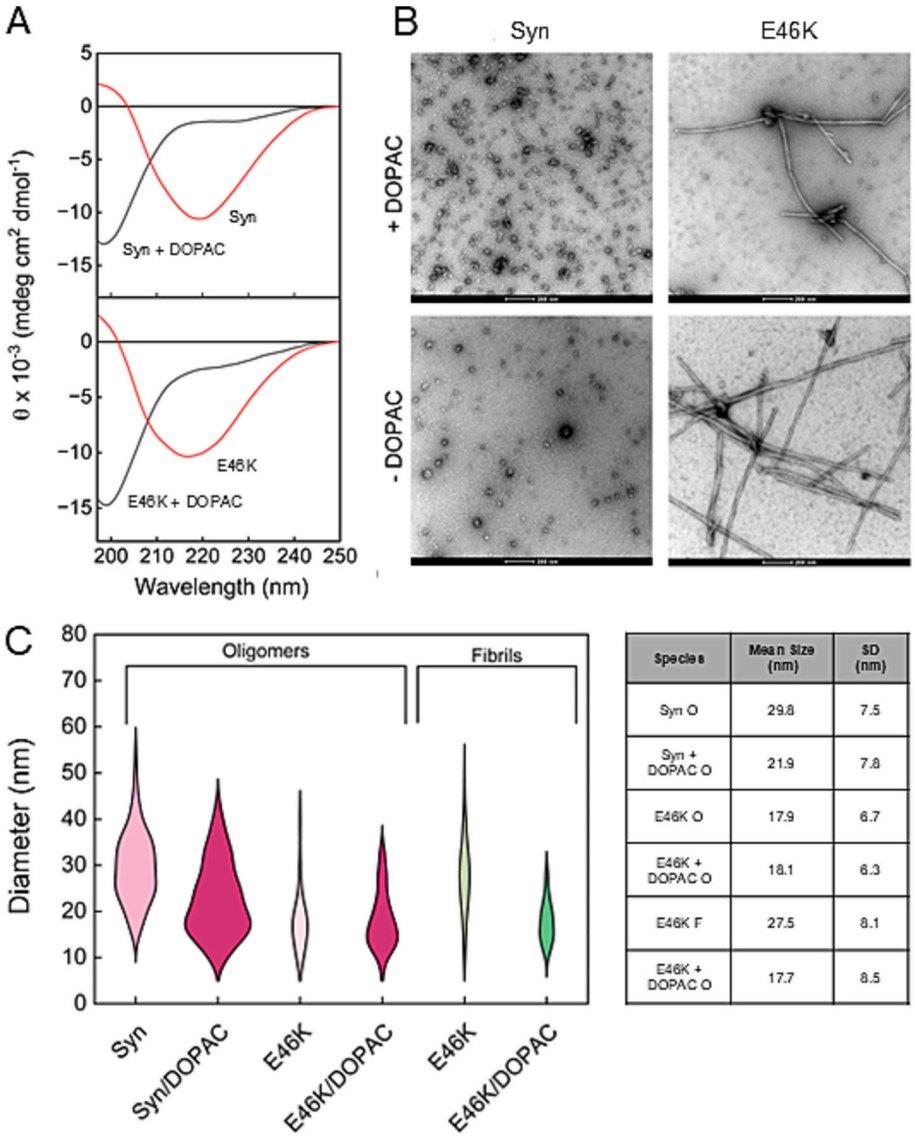

Species	Mean Size (nm)	SD (nm)
Syn O	29.8	7.5
Syn + DOPAC O	21.9	7.8
E46K O	17.9	6.7
E46K + DOPAC O	18.1	6.3
E46K F	27.5	8.1
E46K + DOPAC O	17.7	8.5

Fig. 1. Structural and morphological characterization of Syn and E46K aggregates in the presence and absence of DOPAC. (A) Far-UV CD spectra of Syn and E46K incubated in the absence (red line) or presence of DOPAC (black line, protein/DOPAC 1:5) for 72 h. (B) Representative TEM images of Syn and E46K aggregates formed with or without DOPAC after 72 h incubation. (C) Diameter distribution of Syn and E46K oligomers measured from ≥ 100 particles taken from TEM micrographs (left). Summary table reporting mean diameters (± SD) of oligomeric and fibrillar species observed under the indicated conditions (right).

copper grid (400-square mesh) (TAAB-Laboratories Equipment Ltd., Berks, UK), dried, and negatively stained with a drop of uranyl acetate solution (1%, *w/v*) for 30 s. The excess sample was blotted off with a filter paper, and the grids were washed with distilled water. TEM pictures were taken on a Tecnai G2 12 Twin instrument (FEI Company, Hillsboro, OR), operating at an excitation voltage of 100 kV. Size distribution of protein samples was calculated on an average of 100 particles manually extracted from approximately eight representative TEM micrographs per condition using ImageJ software. Only clearly defined spherical and isolated particles were selected. Measurements were provided with a standard deviation.

2.9. Statistical analysis

All data were reported as mean values ± standard deviation (SD) of triplicates. Statistical analysis using one-way ANOVA, with *p*-value <0.05 as regarded statistically significant. The differences between control and experimental samples were determined by *t*-test.

3. Results

First, we characterized the protein samples incubated in the presence and absence of DOPAC. Far-UV CD spectroscopy showed that DOPAC does not induce detectable conformational changes in the monomeric proteins at time 0, consistent with previous reports [22,23]. Indeed, both Syn and E46K maintained the unfolded/disordered structure

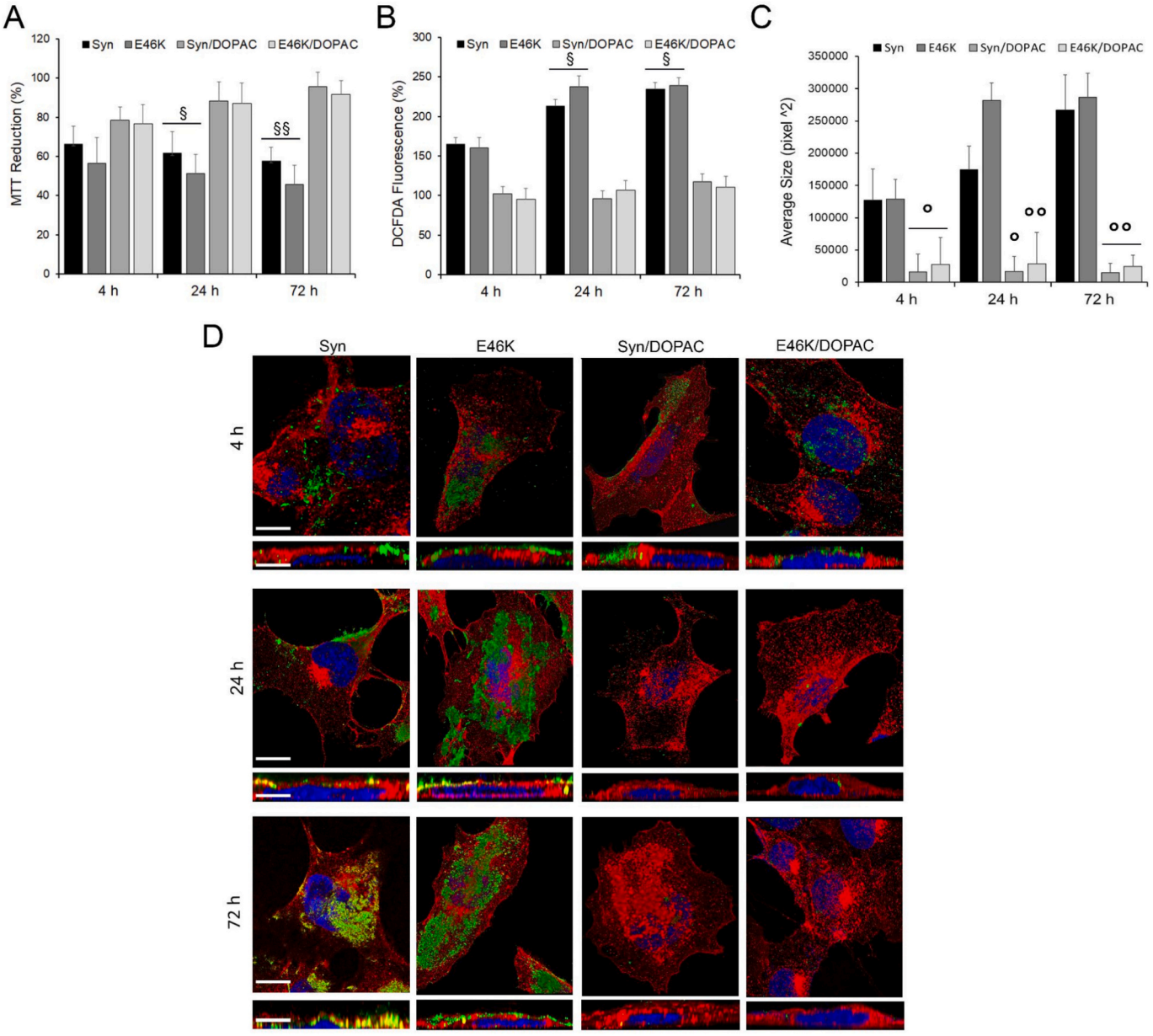

Fig. 2. DOPAC attenuates the formation of cytotoxic synuclein species. SH-SY5Y cells were treated for 4, 24 and 72 h with different Syn aggregates at the final concentrations of 5 μM (monomer equivalent). (A) Mitochondrial activity was assessed by MTT reduction assay. (B) ROS levels were detected by CH2-DCFDA fluorescent probe. Data are expressed as mean ± SE of 3 independent experiments performed in triplicates. Statistical analysis: § $p < 0.05$ vs 4 h to 24 h or 72 h of treatment. (C) Mean aggregate size ± SE measured by 5 STED confocal images for sample. Statistical analysis: ° $p < 0.05$; °° $p < 0.01$ vs aggregates obtained in absence of DOPAC. (D) Representative STED images and 3D reconstructions from z-stack analysis. Nuclei were stained with HOECHST 33342 (blue), plasma membrane with WGA (red) and Syn aggregates with Alexa-514-conjugate anti-Syn antibodies (green). Scale bar: 10 μm (STED images) and 5 μm (3D reconstruction).

previously reported in the absence of the catechol. Upon incubation with DOPAC (protein/DOPAC 1:5) up to 72 h, the CD spectra confirmed the persistence of the disordered structure (Fig. 1A, black line). On the contrary, when incubated for the same time in a buffer at pH 7.5, without DOPAC, both Syn and E46K underwent a conformational transition from random coil to β-sheet structure, as indicated by the appearance of the characteristic negative minimum near 218 nm (Fig. 1A, red line).

The aggregation state of Syn and E46K was further investigated by transmission electron microscopy (TEM) under the same conditions. It should be noted that the aggregation conditions and incubation times employed in this study were selected to preferentially enrich oligomeric species, which are known to coexist in dynamic equilibrium with fibrillar forms during the early stages of α-synuclein aggregation. After 72 h, in the presence of DOPAC (protein/DOPAC 1:5), Syn formed mainly small spherical oligomers with an average diameter of 21.8 ± 7.8 nm, while fibrillar aggregates were not detected at this stage. These oligomers appeared slightly smaller than those formed in the absence of DOPAC (29.8 ± 7.5 nm). Similarly, in the presence of DOPAC, E46K produced spherical oligomers with a mean diameter of 18.1 ± 6.3 nm, smaller than Syn oligomers, although occasional fibrils were also observed (17.7 ± 8.5 nm). In the absence of DOPAC, E46K oligomers exhibited comparable morphology and size (17.9 ± 6.7 nm), whereas fibrils were more abundant and displayed larger diameters (27.5 ± 8.1 nm) compared to those obtained in the presence of the catechol (Fig. 1B-D). The partial coexistence of oligomers and fibrils observed for the E46K mutant in the presence of DOPAC likely reflects the reduced ability of catechols to fully suppress fibrillogenesis in this variant, as previously reported.

We next evaluated the cytotoxic effects of Syn and E46K aggregates obtained in vitro, in the absence or presence of DOPAC, on undifferentiated human neuroblastoma SH-SY5Y cells, following 4 and 24 h of incubation. Cell viability was assessed by MTT assay, while intracellular reactive oxygen species (ROS) production was measured using the fluorescent ROS probe (DCFDA). In the absence of DOPAC, Syn aggregates, and especially those formed by the E46K mutant, induced a significant reduction in cell viability and mitochondrial function (Fig. 2A), accompanied by a significant increase in ROS levels (Fig. 2B), indicative of enhanced oxidative stress. These results are consistent with the well-documented propensity of Syn aggregates to form membrane-associated species in cellular models [26]. Notably, cytotoxicity progressed in a time-dependent manner, with cell viability decreasing by approximately 30% after 4 h and by ~45% after 24 h and 72 h of incubation, while ROS levels increased by about 1.5-fold at 4 h and ~ 2.4-fold at 24 h and 72 h of treatment (Fig. 2A, B).

The E46K mutation in Syn significantly enhances its interaction with cell membrane, compared to the wild-type form, an effect observable as early as 4 h after incubation with cells (Fig. 2D). This observation is consistent with previous studies showing that E46K increases Syn's binding affinity to phospholipids and membranes, likely due to structural changes such as additional hydrogen bonding and modified electrostatic interactions [26,27]. After 24 h of incubation, wild-type Syn also exhibits robust membrane interaction, as indicated by colocalisation analysis (yellow merge). However, cells exposed to E46K display an extensive network of aggregated protein. This suggests that E46K not only binds more strongly to membranes but also promotes aggregation and recruitment of additional E46K molecules into larger assemblies over time.

Aggregate size analysis by STED confocal microscopy (Fig. 2C) confirmed that both Syn and E46K form aggregates larger than their DOPAC-treated counterparts, with the effect being particularly pronounced for E46K. The reduced size of DOPAC-containing aggregates suggests a greater likelihood of their internalization and clearance by cellular proteostatic mechanisms. Importantly, STED analysis performed after prolonged incubation (72 h) revealed aggregate distributions and sizes comparable to those observed at 24 h, indicating that no further accumulation or enlargement of DOPAC-modified aggregates occurs over time.Consistently, cells treated with Syn or E46K aggregates grown in the presence of DOPAC showed partial rescue of mitochondrial function (Fig. 2A) and reduced ROS production (Fig. 2B), effects that were maintained at 72 h. These findings are in line with previous evidence indicating that DOPAC stabilizes Syn monomers and promotes the formation of small, non-fibrillar oligomers (dimers and trimers) resistant to fibrillation and membrane disruption [26].

Moreover, immunofluorescence analysis revealed a marked reduction of Syn/DOPAC or E46K/DOPAC aggregates at the cell membrane after 24 h of cell treatment (Fig. 2C). This pattern was preserved at 72 h and correlated with the absence of detectable cytotoxicity (Fig. 2A,B) in these samples, supporting the hypothesis that DOPAC-containing aggregates exhibit lower affinity for the plasmamembrane. Such species may either fail to bind membrane, bind with reduced strength, or be more efficiently r removed from the cell surface via endocytic or autophagic process.

Previous evidence indicates that Syn degradation engages both ubiquitin–proteasome and autophagy–lysosomal systems [13,28]. To dissect their respective contributions, we employed selective inhibitors of the proteasome and autophagy and examined their effects on Syn accumulation and the ensuing cellular responses, in order to clarify their roles in maintaining Syn homeostasis. In our experimental model, treatment with the proteasome inhibitor MG132 resulted in reduced cell viability and increased ROS production in cells exposed to E46K/DOPAC aggregates (Fig. 3A, B). This indicates that these aggregates are normally processed by the proteasome. Consistently, STED microscopy revealed a marked accumulation of internalized aggregates upon MG132 treatment (Fig. 3C), further supporting a central role of the UPS in E46K/DOPAC aggregate clearance. The build-up of aggregates under proteasome inhibition suggests impaired degradation and intracellular accumulation, leading to cellular stress. By contrast, no significant changes in cell viability or ROS production were observed in cells treated with Syn/DOPAC aggregates in the presence of MG132, compared to untreated controls. This implies that these aggregates are primarily degraded through alternative mechanisms, likely autophagic pathways rather than the proteasome.

In the presence of chloroquine (CQ), which blocks autophagosome, lysosome fusion and thereby impairs autophagic flux (ALP), the toxicity of Syn, Syn/DOPAC, and E46K aggregates was generally increased (Fig. 3D, E). This effect can be attributed to the impaired clearance of toxic protein aggregates by autophagy, leading to lysosomal dysfunction and the intracellular accumulation of autophagosomes. Such build-up exacerbates the cellular stress and toxicity associated with synuclein aggregates. Mechanistically, CQ primarily impairs autophagy by preventing autophagosome, lysosome fusion, rather than by directly altering lysosomal pH or hydrolase activity. This blockade disrupts lysosomal function, affects the *endo*-lysosomal system and Golgi apparatus, and further enhances aggregate accumulation and cellular stress. Consistently, STED microscopy confirmed the presence of numerous intracellular aggregates in CQ-treated cells (Fig. 3F).

Interestingly, the toxicity profile of E46K/DOPAC conjugates differed from that of Syn and Syn/DOPAC aggregates. While CQ treatment enhanced the toxicity of Syn and Syn/DOPAC species, cells exposed to E46K/DOPAC conjugates showed reduced toxicity under CQ compared to untreated controls, though still higher than in cells treated with the proteasome inhibitor MG132. This finding suggests a more complex interplay between degradation pathways in the handling of DOPAC-modified species. One plausible explanation is that E46K/DOPAC conjugates may rely less on autophagy and more on proteasome-mediated clearance when autophagy is inhibited. Thus, CQ-induced disruption of autophagic flux appears to shift the balance between proteostatic pathways, differentially affecting the processing and toxicity of Syn and E46K aggregates.

In our experimental conditions utilizing SH-SY5Y cells treated for 4 h with either Syn or E46K mutant form, the application of the proteasomal

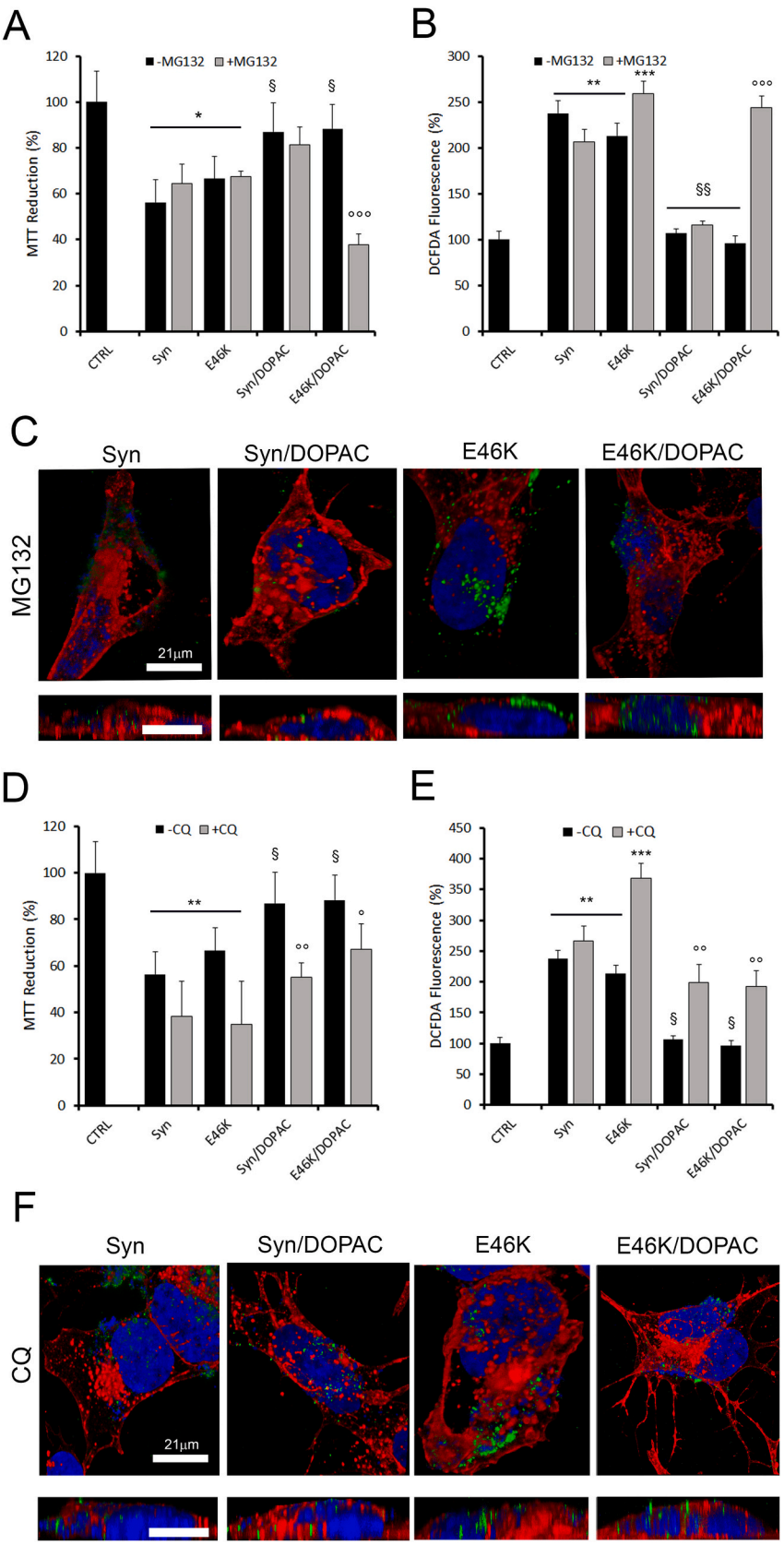

(caption on next page)

Fig. 3. Proteasome and autophagy pathways contribute differently to the clearance and toxicity of α-synuclein aggregates. SH-SY5Y cells were pre-treated for 16 h with proteasome (MG132) and autophagy (Chloroquine, CQ) inhibitors before the treatment for further 4 h with different protein aggregates at the final concentrations of 5 μM (monomer concentration). Mitochondrial activities were analyzed in terms of MTT reduction (A, D) and ROS production detected by CH2-DCFDA probe (B, E). Data were reported as the mean of 3 independent experiments performed in triplicates ± SE. Statistical analysis: * $p < 0.05$; ** $p < 0.01$; *** $p < 0.001$ vs untreated cells (CTRL); ° $P < 0,05$; °° $P < 0,01$; °°° $P < 0,001$ respect to cells no-treated with MG132 or CQ; § $p < 0,05$; §§ $p < 0,01$ vs Syn and E46K without DOPAC. C, F) Representative STED images and 3D reconstructions of the z-stack analysis. Cells were labeled with HOECHST 33342 (blue, nuclei), WGA (red, membrane) and anti-Syn with Alexa-514 conjugate antibodies (green). Scale bar of 3D reconstruction is 6 μm.

inhibitor MG132 resulted in a notable increase in the size and number of LAMP1-positive lysosomal structures (Fig. 4A). LAMP1, a lysosomal-associated membrane protein commonly used as a lysosomal marker, identifies compartments whose enlargement or clustering reflects lysosomal expansion. Despite this, LAMP1-positive compartments are functionally heterogeneous, and the observed increase most likely indicates an enhanced lysosomal involvement in the clearance of protein aggregates upon proteasomal inhibition. Notably, this lysosomal expansion was absent in cells treated with Syn or E46K aggregates formed in the presence of DOPAC, indicating that DOPAC may modulate lysosomal dynamics in response to proteostatic stress (Fig. 4A).

Further supporting this view, Fig. 3B shows that cells treated with E46K aggregates assembled in the presence of DOPAC exhibit a prominent cage-like area filled with numerous LAMP1-positive puncta surrounding the protein aggregates. This morphology suggests effective targeting of the aggregates to lysosomes for degradation. This hypothesis is quantitatively supported by Manders' colocalization coefficient, which shows a high degree of overlap between Syn aggregates and LAMP1, confirming their lysosomal localization. These findings reinforce the role of DOPAC in promoting lysosomal clearance of E46K aggregates.

In parallel, analysis of lysosomal-associated membrane protein 2 (LAMP2), particularly the LAMP2A isoform involved in chaperone-mediated autophagy (CMA), revealed a high degree of colocalization with Syn and E46K aggregates in cells not treated with DOPAC (Fig. 4C). This suggests that, under basal conditions, these aggregates are preferentially targeted to lysosomes via CMA, with LAMP2A acting as a receptor for selective cargo recognition and translocation. Interestingly, cells exposed to E46K aggregates formed in the presence of DOPAC showed a marked reduction in LAMP2A colocalization, implying a potential shift in the route of lysosomal degradation, potentially from CMA to macroautophagy or alternative lysosomal pathways.

To further investigate the autophagic response, we examined autophagosome turnover by assessing the levels of p62, a selective autophagy receptor whose accumulation indicates impaired autophagic flux. Immunofluorescence analysis revealed elevated p62 levels in cells treated with Syn and E46K aggregates at both 4- and 24-h post-treatment, consistent with defective autophagosome clearance and autophagic stress (Fig. 4D). In contrast, cells treated with DOPAC-derived aggregates did not show p62 accumulation, pointing to a more efficient aggregates clearance mechanism, likely via enhanced autophagy. These findings collectively support a protective role for DOPAC in facilitating lysosomal and autophagic degradation of Syn and E46K aggregates, thereby mitigating aggregate-induced proteostatic stress.

4. Discussion

Our study provides important insights into the distinct cytotoxicity and intracellular processing of wild-type and E46K Syn aggregates, as well as the modulatory role of DOPAC on their toxicity and cellular handling.

The DOPAC concentration used in this study (25 μM; protein/DOPAC ratio 1:5) was chosen on the basis of previous in vitro studies demonstrating effective modulation of α-synuclein aggregation and cytotoxicity. Importantly, reported extracellular DOPAC concentrations in dopaminergic brain regions, such as the striatum in rodent models, are in the low micromolar range under basal conditions, as determined by in vivo microdialysis (e.g., ~10.7 μM). While the concentration employed here is somewhat higher than basal extracellular levels, it remains within the same order of magnitude and therefore supports the physiological plausibility of the observed effects, at least in the context of proof-of-principle investigations. Future studies will be necessary to establish whether similar modulatory activity is preserved at strictly physiological DOPAC concentrations in vivo [29].

The results show that Syn aggregates, especially those harbouring the E46K mutation, induce marked, time dependent cytotoxic effects in SH-SY5Y neuroblastoma cells. These effects include reduced mitochondrial viability and increased ROS production, consistent with oxidative stress arising from aggregate–membrane interactions. This observation aligns with previous studies indicating that the E46K mutation enhances Syn's membrane-binding propensity through altered electrostatic and hydrogen-bonding profiles [26]. Our colocalization analyses confirm and suggest that this membrane engagement fosters the nucleation and recruitment of additional Syn molecules amplifying aggregate propagation and neuronal toxicity.

Importantly, the presence of DOPAC during Syn and E46K aggregation promotes the formation of a DOPAC–protein complex with markedly reduced toxicity and ROS production. This suggests that DOPAC stabilizes Syn in conformations less prone to membrane interaction and fibrillation. The reduced membrane association and cytotoxicity of DOPAC-containing aggregates likely reflect their altered biophysical properties, smaller oligomeric states, and lower affinity for cellular membranes, or enhanced clearance through cellular degradation pathways. Importantly, control experiments in which SH-SY5Y cells were treated with DOPAC alone did not reveal detectable changes in basal autophagy markers (p62/SQSTM1 and LC3-II), indicating that DOPAC at the concentration used does not directly modulate the autophagic machinery; rather, its effects on cellular clearance pathways are likely mediated indirectly through DOPAC-induced structural remodeling of α-synuclein aggregates.

The degradation of misfolded Syn aggregates is known to involve multiple proteostasis systems, including the UPS, CMA, and the ALP. Our data confirm this complexity. Inhibition of the proteasome with MG132 led to increased cytotoxicity and ROS levels in cells treated with E46K/DOPAC aggregates, but not with Syn/DOPAC aggregates, suggesting that the E46K/DOPAC species are primarily degraded via the UPS. This interpretation is reinforced by STED microscopy, which revealed intracellular accumulation of E46K/DOPAC aggregates under proteasome inhibition.

In contrast, inhibition of ALP with chloroquine (CQ) increased toxicity in cells treated with all Syn-derived aggregates, though to varying degrees. The unexpected finding that CQ treatment reduced the toxicity of E46K/DOPAC aggregates, compared to untreated conditions, points to a complex compensatory relationship between the autophagic and proteasomal systems. It is possible that in the absence of autophagy, these conjugates are redirected to proteasomal degradation more efficiently. This functional redundancy in degradation pathways highlights the adaptive nature of cellular proteostasis mechanisms and the importance of context in aggregate clearance.

Several studies provide mechanistic support for models in which autophagy inhibition alters UPS activity or substrate routing, thereby contextualizing our observations. CQ is a well-established late-stage autophagy inhibitor that blocks autophagosome–lysosome fusion, leading to the accumulation of LC3-II and p62/SQSTM1 [30]. Such inhibition increases the burden of ubiquitinated substrates that would

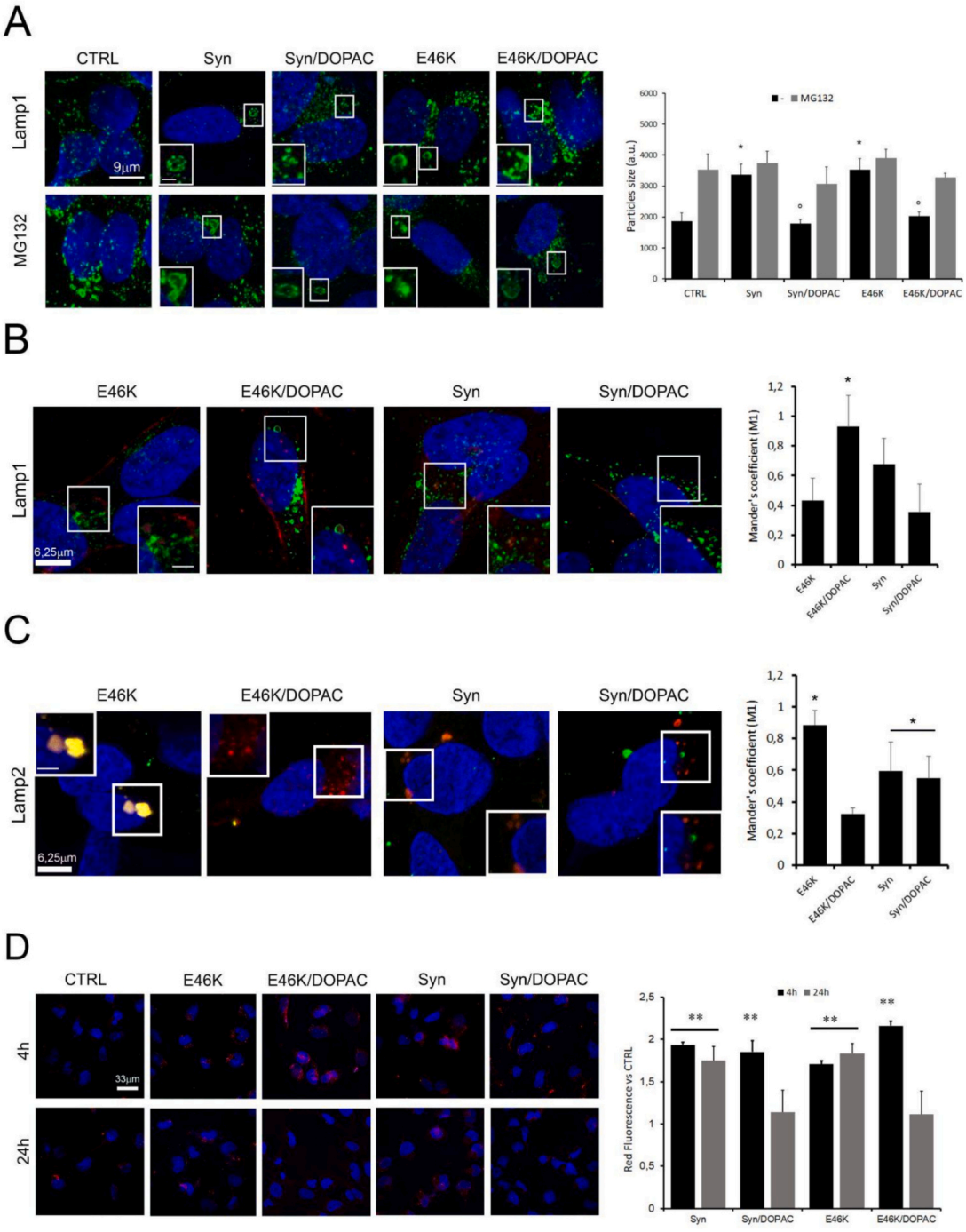

Fig. 4. Aggregate trafficking and lysosomal response upon proteasome inhibition. SH-SY5Y cells were treated with different protein aggregates (final concentration: 5 μM, expressed as monomer equivalent) for 4 h. (A) SH-SY5Y cells were pre-treated for 16 h with the proteasome inhibitor MG132 prior to exposure to different protein aggregates for 4 h. Representative confocal microscopy images showing LAMP1 (green) and nuclei (blue) staining. A selected region in each image is highlighted by a frame, and an enlarged view is shown in the bottom-left corner Scale bar:1.8 μm. The right panel displays the quantification of lysosome sizes, analyzed using ImageJ software. Statistical analysis: $*p < 0.05$ vs. untreated control cells (CTRL); °p < 0.05 vs. Syn and E46K alone. (B) Representative confocal microscopy images showing LAMP1 (green), nuclei (blue), and protein aggregates (red). A selected region in each image is highlighted by a frame, and an enlarged view is shown in the bottom-right corner Scale bar: 3 μm. Colocalization analysis is presented in the graph on the right, reported as Mander's coefficient. ImageJ software was used for quantification. Statistical analysis: *p < 0.05 vs. E46K. C) Representative confocal microscopy images showing LAMP2 (green), nuclei (blue) staining and protein aggregates (red). A selected region in each image is highlighted by a frame, and an enlarged view is shown in the top-left corner Scale bar: 3 μm. The right panel displays the quantification of lysosome sizes, analyzed using ImageJ software. Statistical analysis: *p < 0.05 vs. untreated control cells (CTRL); °p < 0.05 vs. Syn and E46K alone. D) SH-SY5Y cells were treated for 4 or 24 h with 72-h aggregates of Syn or E46K, either in the absence or presence of DOPAC. Representative confocal images show p62 staining (red) and nuclear staining (blue). The graph on the right displays the mean fluorescence intensity of the p62 signal relative to untreated control cells (CTRL). Semi-quantitative analysis was performed using ImageJ software as integrated intensity from at least three images per condition, across three independent experiments. Data are expressed as the mean ± SE of $n = 3$ independent experiments, each conducted in triplicate. Statistical analysis: $**p < 0.01$ vs. untreated control cells (CTRL).

normally be processed via autophagy, potentially shifting their clearance toward the UPS.

Moreover, extensive evidence demonstrates tight cross-talk between the UPS and autophagic pathways, whereby impairment of one system can trigger compensatory activation or reprogramming of the other [31–33]. These adaptive responses may involve changes in proteasomal flux, altered ubiquitin availability, or stress-induced upregulation of proteasome biogenesis. Importantly, α-synuclein, both wild-type and E46K, is known to be degraded by multiple proteostatic routes, and its ubiquitination state plays a critical role in determining its targeting toward the UPS, macroautophagy, or chaperone-mediated autophagy (CMA) [34]. Recent studies further indicate that distinct ubiquitin signatures govern α-synuclein fate and clearance efficiency [35].

Although proteasome activity, proteasomal subunit expression, and α-synuclein ubiquitination were not directly assessed in the present study, these mechanisms offer a biologically plausible framework for the CQ-mediated reduction in E46K/DOPAC toxicity. Collectively, our findings support the hypothesis that, under conditions of autophagy inhibition, E46K/DOPAC aggregates may be preferentially redirected toward UPS-dependent degradation.

Lysosomal involvement was further confirmed through increased LAMP1-positive structures in MG132-treated cells exposed to Syn and E46K aggregates. The presence of large, punctate lysosomal structures may reflect compensatory lysosomal activation under proteasomal stress. However, this response was attenuated in cells treated with DOPAC-containing aggregates, indicating either less burden on lysosomal systems or more efficient clearance. These findings are consistent with recent studies emphasizing the critical roles of LAMP1 and LAMP2 in lysosomal integrity and autophagic flux. LAMP1 and LAMP2 participate in autophagosome–lysosome fusion, a crucial step for degrading protein aggregates such as Syn. When Syn aggregates accumulate, a failure in lysosomal degradation leads to impaired autophagic flux, reflected by abnormal levels of LAMP proteins and increased accumulation of the autophagy receptor protein p62 [36,37].

Manders' coefficient analysis revealed that E46K/DOPAC aggregates are effectively sequestered within LAMP1-positive lysosomal structures but show reduced colocalization with LAMP2A. This suggests that while these aggregates are targeted to lysosomes, their degradation may occur independently of CMA, possibly via macroautophagy. In contrast, Syn and E46K aggregates formed without DOPAC colocalize strongly with LAMP2A, supporting their degradation via CMA. These observations corroborate the findings by Parcon et al. (2018), which highlight the selective role of LAMP2A in CMA-mediated degradation of Syn. Impairments in this pathway can result in reduced lysosomal clearance and progressive neurodegeneration [38].

Moreover, accumulation of p62 was observed in cells treated with Syn and E46K aggregates, indicating impaired autophagosome turnover. This accumulation reflects lysosomal stress and inefficient clearance mechanisms, in line with prior observations showing a correlation between increased p62 levels and disrupted lysosomal function [37,39]. However, p62 levels remained unchanged in cells exposed to DOPAC-containing aggregates, suggesting that these assemblies do not disrupt autophagic flux and are more efficiently processed. Interestingly, pharmacological agents such as treh15alose have been shown to restore lysosomal function and reduce p62 accumulation, offering therapeutic perspectives in α-synucleinopathies [40]. Our findings suggest that DOPAC may exert a similar effect by facilitating aggregate clearance and preserving lysosomal homeostasis.

5. Conclusion

In summary, our study demonstrates that DOPAC significantly modulates the structural, toxicological, and intracellular trafficking properties of both wild-type and E46K Syn aggregates. While E46K aggregates are inherently more toxic and membrane-active, their conjugation with DOPAC attenuates these effects and redirects their degradation toward more efficient pathways. These results underline the therapeutic potential of small molecules like DOPAC in modulating Syn aggregation and toxicity, especially in the context of familial Parkinson's disease mutations. The integrated evidence also reinforces the central role of lysosomal function and its key players, LAMP1, LAMP2A, and p62, in the handling of Syn aggregates, further highlighting the relevance of maintaining proteostasis in neurodegenerative disease intervention.

6. Study limitations and future perspectives

While this study provides novel insights into the ability of DOPAC to modulate α-synuclein aggregation and toxicity in SH-SY5Y cells, several limitations should be acknowledged. A major limitation is the exclusive use of undifferentiated SH-SY5Y neuroblastoma cells. Although this model is widely used and well characterized for investigating α-synuclein aggregation, cytotoxicity, and clearance pathways, offering advantages such as high reproducibility and a human-derived background, it does not recapitulate key physiological properties of mature neurons. In particular, undifferentiated SH-SY5Y cells lack synaptic specialization and neurotransmission-related functions, precluding the assessment of how DOPAC may influence synaptic vesicle dynamics, SNARE complex assembly, or neurotransmitter release. Consequently, the cellular responses to α-synuclein aggregates and DOPAC observed here may not fully reflect those occurring in dopaminergic neurons in vivo.

Another important limitation is the focus on the E46K α-synuclein mutant. Parkinson's disease encompasses multiple pathogenic variants (e.g., A30P, A53T), as well as sporadic cases involving wild-type or post-translationally modified α-synuclein species, raising uncertainty regarding the extent to which the modulatory effects of DOPAC can be generalized across different pathological forms. These considerations underscore the need to validate the present findings in more physiologically relevant systems, including differentiated SH-SY5Y cells, primary midbrain neurons, human iPSC-derived dopaminergic neurons, brain organoids, and animal models of Parkinson's disease.

A further limitation of the present study is the use of a single protein/DOPAC molar ratio and DOPAC concentration. Although the concentration employed falls within the same order of magnitude as extracellular DOPAC levels reported in dopaminergic brain regions, a comprehensive dose–response analysis will be required to define the full spectrum of DOPAC modulatory activity and to determine whether comparable effects are maintained at strictly physiological concentrations.

At the molecular level, the precise structural determinants underlying the interaction between DOPAC and α-synuclein aggregates remain to be elucidated. Advanced structural approaches, such as high-resolution NMR spectroscopy or cryo-electron microscopy, will be essential to characterize DOPAC-induced conformational changes, identify specific binding sites, and clarify the mechanisms by which DOPAC stabilizes less toxic aggregate species and reduces membrane association.

In addition, the present work focuses on acute cellular responses and therefore does not address the long-term consequences of sustained DOPAC exposure. Extended studies will be necessary to evaluate chronic effects on neuronal function, proteostasis, and behaviour, particularly in in vivo models.

Finally, the interplay observed here between distinct protein quality control pathways, including the proteasome, macroautophagy, and chaperone-mediated autophagy, warrants further investigation. A deeper understanding of how cells dynamically coordinate these degradation systems in response to toxic α-synuclein species may inform future strategies aimed at restoring proteostatic balance in synucleinopathies.

Collectively, addressing these limitations through complementary cellular, structural, and in vivo approaches will be critical for advancing DOPAC-based strategies and for translating the present findings into

meaningful therapeutic progress for Parkinson's disease and related synucleinopathies.

Contribution statement

The authors declare that they have no known competing financial interests or personal relationships that could have appeared to influence the work reported in this paper.

CRediT authorship contribution statement

Manuela Leri: Validation, Methodology, Investigation, Formal analysis. **Philipp Trolese:** Validation, Methodology, Investigation, Formal analysis. **Ilenia Inciardi:** Methodology, Formal analysis, Data curation. **Patrizia Polverino de Laureto:** Writing – review & editing, Writing – original draft, Conceptualization. **Monica Bucciantini:** Writing – review & editing, Writing – original draft, Supervision, Resources, Conceptualization.

Declaration of competing interest

The authors declare that they have no known competing financial interests or personal relationships that could have appeared to influence the work reported in this paper.

Acknowledgements

This work was also supported by a grant from the University of Florence (Fondi di Ateneo 2022-24 to Monica Bucciantini). We thank MIUR-Italy ("Progetto Dipartimenti di Eccellenza 2023-2027" allocated to Department of Experimental and Clinical Biomedical Sciences "Mario Serio").

Data availability

Data will be made available on request.

References

[1] E. Hallacli, C. Kayatekin, S. Nazeen, X.H. Wang, Z. Sheinkopf, S. Sathyakumar, S. Sarkar, X. Jiang, X. Dong, R. Di Maio, W. Wang, M.T. Keeney, D. Felsky, J. Sandoe, A. Vahdatshoar, N.D. Udeshi, D.R. Mani, S.A. Carr, S. Lindquist, V. Khurana, The Parkinson's disease protein alpha-synuclein is a modulator of processing bodies and mRNA stability, Cell 185 (12) (2022) 2035–2056, e33.

[2] O. Lucas-Jiménez, N. Ibarretxe-Bilbao, I. Diez, J. Peña, B. Tijero, M. Galdós, A. Murueta-Goyena, R. Del Pino, M. Acera, J.C. Gómez-Esteban, I. Gabilondo, N. Ojeda, Brain degeneration in synucleinopathies based on analysis of cognition and other nonmotor features: a multimodal imaging study, Biomedicines 11 (2) (2023).

[3] M. Pantazopoulou, V. Brembati, A. Kanellidi, L. Bousset, R. Melki, L. Stefanis, Distinct alpha-Synuclein species induced by seeding are selectively cleared by the Lysosome or the Proteasome in neuronally differentiated SH-SY5Y cells, J. Neurochem. 156 (6) (2021) 880–896.

[4] I. Choi, Y. Zhang, S.P. Seegobin, M. Pruvost, Q. Wang, K. Purtell, B. Zhang, Z. Yue, Microglia clear neuron-released α-synuclein via selective autophagy and prevent neurodegeneration, Nat. Commun. 11 (1) (2020) 1386.

[5] P. Parekh, N. Sharma, M. Sharma, A. Gadepalli, A.A. Sayyed, S. Chatterjee, A. Kate, A. Khairnar, AMPK-dependent autophagy activation and alpha-Synuclein clearance: a putative mechanism behind alpha-mangostin's neuroprotection in a rotenone-induced mouse model of Parkinson's disease, Metab. Brain Dis. 37 (8) (2022) 2853–2870.

[6] Y.T. Wang, J.H. Lu, Chaperone-mediated autophagy in neurodegenerative diseases: molecular mechanisms and pharmacological opportunities, Cells 11 (14) (2022).

[7] R.A. Nixon, D.C. Rubinsztein, Mechanisms of autophagy-lysosome dysfunction in neurodegenerative diseases, Nat. Rev. Mol. Cell Biol. 25 (11) (2024) 926–946.

[8] P. Maiti, J. Manna, G.L. Dunbar, Current understanding of the molecular mechanisms in Parkinson's disease: Targets for potential treatments, Transl Neurodegener 6 (2017) 28.

[9] C. Pitcairn, N. Murata, A.J. Zalon, I. Stojkovska, J.R. Mazzulli, Impaired autophagic-lysosomal fusion in Parkinson's patient midbrain neurons occurs through loss of ykt6 and is rescued by farnesyltransferase inhibition, J. Neurosci. 43 (14) (2023) 2615–2629.

[10] G.K. Tofaris, R. Layfield, M.G. Spillantini, Alpha-synuclein metabolism and aggregation is linked to ubiquitin-independent degradation by the proteasome, FEBS Lett. 509 (1) (2001) 22–26.

[11] L. Zondler, M. Kostka, P. Garidel, U. Heinzelmann, B. Hengerer, B. Mayer, J. H. Weishaupt, F. Gillardon, K.M. Danzer, Proteasome impairment by α-synuclein, PLoS One 12 (9) (2017) e0184040.

[12] C. McKinnon, M.L. De Snoo, E. Gondard, C. Neudorfer, H. Chau, S.G. Ngana, D. M. O'Hara, J.M. Brotchie, J.B. Koprich, A.M. Lozano, L.V. Kalia, S.K. Kalia, Early-onset impairment of the ubiquitin-proteasome system in dopaminergic neurons caused by α-synuclein, Acta Neuropathol. Commun. 8 (1) (2020) 17.

[13] M. Xilouri, T. Vogiatzi, K. Vekrellis, D. Park, L. Stefanis, Abberant alpha-synuclein confers toxicity to neurons in part through inhibition of chaperone-mediated autophagy, PLoS One 4 (5) (2009) e5515.

[14] F. Yang, Y.P. Yang, C.J. Mao, L. Liu, H.F. Zheng, L.F. Hu, C.F. Liu, Crosstalk between the proteasome system and autophagy in the clearance of α-synuclein, Acta Pharmacol. Sin. 34 (5) (2013) 674–680.

[15] J. Pan, A. Dalzini, N.K. Khadka, C.M. Aryal, L. Song, Lipid extraction by α-synuclein generates semi-transmembrane defects and lipoprotein nanoparticles, ACS Omega 3 (8) (2018) 9586–9597.

[16] M. Stöckl, P. Fischer, E. Wanker, A. Herrmann, Alpha-synuclein selectively binds to anionic phospholipids embedded in liquid-disordered domains, J. Mol. Biol. 375 (5) (2008) 1394–1404.

[17] C. Galvagnion, A.K. Buell, G. Meisl, T.C. Michaels, M. Vendruscolo, T.P. Knowles, C.M. Dobson, Lipid vesicles trigger α-synuclein aggregation by stimulating primary nucleation, Nat. Chem. Biol. 11 (3) (2015) 229–234.

[18] A.P. Pandey, F. Haque, J.C. Rochet, J.S. Hovis, α-Synuclein-induced tubule formation in lipid bilayers, J. Phys. Chem. B 115 (19) (2011) 5886–5893.

[19] S. Mansueto, G. Fusco, A. De Simone, α-Synuclein and biological membranes: the danger of loving too much, Chem. Commun. (Camb.) 59 (57) (2023) 8769–8778.

[20] A. Mori, Y. Imai, N. Hattori, Lipids: Key Players That Modulate α-Synuclein Toxicity and Neurodegeneration in Parkinson's Disease, Int. J. Mol. Sci. 21 (9) (2020).

[21] L. Palazzi, B. Fongaro, M. Leri, L. Acquasaliente, M. Stefani, M. Bucciantini, P. Polverino de Laureto, Structural Features and Toxicity of α-Synuclein Oligomers Grown in the Presence of DOPAC, Int. J. Mol. Sci. 22 (11) (2021).

[22] I. Inciardi, E. Rizzotto, F. Gregoris, B. Fongaro, A. Sosic, G. Minervini, P. Polverino de Laureto, Catechol-induced covalent modifications modulate the aggregation tendency of α-synuclein: An in-solution and in-silico study, Biofactors 51 (1) (2025) e2086.

[23] B. Fongaro, E. Cappelletto, A. Sosic, B. Spolaore, P. Polverino de Laureto, 3,4-Dihydroxyphenylethanol and 3,4-dihydroxyphenylacetic acid affect the aggregation process of E46K variant of α-synuclein at different extent: Insights into the interplay between protein dynamics and catechol effect, Protein Sci. 31 (7) (2022) e4356.

[24] J. Schindelin, I. Arganda-Carreras, E. Frise, V. Kaynig, M. Longair, T. Pietzsch, S. Preibisch, C. Rueden, S. Saalfeld, B. Schmid, J.Y. Tinevez, D.J. White, V. Hartenstein, K. Eliceiri, P. Tomancak, A. Cardona, Fiji: an open-source platform for biological-image analysis, Nat. Methods 9 (7) (2012) 676–682.

[25] S.C. Gill, P.H. von Hippel, Calculation of protein extinction coefficients from amino acid sequence data, Anal. Biochem. 182 (2) (1989) 319–326.

[26] E. Rizzotto, A. Pierangelini, B. Fongaro, M. Leri, I. Inciardi, P. Trolese, V. De Filippis, M. Bucciantini, L. Acquasaliente, P. Polverino de Laureto, DOPAC as a modulator of α-Synuclein and E46K interactions with membrane: Insights into binding dynamics, Int. J. Biol. Macromol. 294 (2025) 139427.

[27] C.R. Bodner, A.S. Maltsev, C.M. Dobson, A. Bax, Differential phospholipid binding of alpha-synuclein variants implicated in Parkinson's disease revealed by solution NMR spectroscopy, Biochemistry 49 (5) (2010) 862–871.

[28] S. Engelender, α-Synuclein fate: proteasome or autophagy? Autophagy 8 (3) (2012) 418–420.

[29] F.C. Jing, H. Chen, C.L. Li, Rapid determination of dopamine and its metabolites during in vivo cerebral microdialysis by routine high performance liquid chromatography with electrochemical detection, Biomed. Environ. Sci. 20 (4) (2007) 317–320.

[30] M. Mauthe, I. Orhon, C. Rocchi, X. Zhou, M. Luhr, K.J. Hijlkema, R.P. Coppes, N. Engedal, M. Mari, F. Reggiori, Chloroquine inhibits autophagic flux by decreasing autophagosome-lysosome fusion, Autophagy 14 (8) (2018) 1435–1455.

[31] N.M. Kocaturk, D. Gozuacik, Crosstalk Between Mammalian Autophagy and the Ubiquitin-Proteasome System, Front. Cell Dev. Biol. 6 (2018) 128.

[32] J.L. Sun-Wang, S. Ivanova, A. Zorzano, The dialogue between the ubiquitin-proteasome system and autophagy: Implications in ageing, Ageing Res. Rev. 64 (2020) 101203.

[33] Y. Li, S. Li, H. Wu, Ubiquitination-Proteasome System (UPS) and Autophagy Two Main Protein Degradation Machineries in Response to Cell Stress, Cells 11 (5) (2022).

[34] J.Q. Yan, Y.H. Yuan, S.F. Chu, G.H. Li, N.H. Chen, E46K Mutant α-Synuclein Is Degraded by Both Proteasome and Macroautophagy Pathway, Molecules 23 (11) (2018).

[35] D. Zenko, J. Marsh, A.R. Castle, R. Lewin, R. Fischer, G.K. Tofaris, Monitoring α-synuclein ubiquitination dynamics reveals key endosomal effectors mediating its trafficking and degradation, Sci. Adv. 9 (24) (2023) eadd8910.

[36] G.K. Tofaris, Lysosome-dependent pathways as a unifying theme in Parkinson's disease, Mov. Disord. 27 (11) (2012) 1364–1369.

[37] K. Tanji, S. Odagiri, Y. Miki, A. Maruyama, Y. Nikaido, J. Mimura, F. Mori, E. Warabi, T. Yanagawa, S. Ueno, K. Itoh, K. Wakabayashi, p62 Deficiency Enhances α-Synuclein Pathology in Mice, Brain Pathol. 25 (5) (2015) 552–564.

[38] P.A. Parcon, M. Balasubramaniam, S. Ayyadevara, R.A. Jones, L. Liu, R. J. Shmookler Reis, S.W. Barger, R.E. Mrak, W.S.T. Griffin, Apolipoprotein E4 inhibits autophagy gene products through direct, specific binding to CLEAR motifs, Alzheimers Dement. 14 (2) (2018) 230–242.

[39] S. Abounit, L. Bousset, F. Loria, S. Zhu, F. de Chaumont, L. Pieri, J.C. Olivo-Marin, R. Melki, C. Zurzolo, Tunneling nanotubes spread fibrillar α-synuclein by intercellular trafficking of lysosomes, EMBO J. 35 (19) (2016) 2120–2138.

[40] A.C. Hoffmann, G. Minakaki, S. Menges, R. Salvi, S. Savitskiy, A. Kazman, H. Vicente Miranda, D. Mielenz, J. Klucken, J. Winkler, W. Xiang, Extracellular aggregated alpha synuclein primarily triggers lysosomal dysfunction in neural cells prevented by trehalose, Sci. Rep. 9 (1) (2019) 544.